A decorative graphic consisting of three blue circles of varying sizes and three thin blue lines. One large circle is at the top center, a smaller one is below it, and a very large one is at the bottom right. The lines connect the top-left and top-right corners to the top circle, and the bottom-left corner to the middle circle.

## **6. Development of Dry Powder for Inhalation**

Freeze-drying of nanoparticles is not an easy process and requires a comprehensive expertise and understanding of the process. However, one may find that most of papers published in this field studied the freeze-drying of nanoparticles by trial and error, i.e. by trying different conditions of freeze-drying and selecting the best after the analysis of freeze-dried product.

Freeze drying is a complex process because it consists of simultaneous heat and mass transfer. During the primary drying period, the sublimation kinetics are controlled either by heat transfer flux from the shelf and from the surrounding toward the ice sublimation front inside the vial or by water vapor mass transfer through the dried layer. Various methods have been developed to increase the heat and mass transfer rates during freeze drying. Of these, the most common and effective method is the annealing of the frozen sample before freeze drying. The annealing of the sample leads to increase in the ice crystal size and its percentage distribution and hence increase in heat and mass transfer rate (1, 2). Recently, Daoussi et al. (3) have reported that the presence of organic solvents such as tertiary butanol in the formulation increases the primary drying rate as compared to the pure water-based system. Nevertheless, the freeze-drying process generates various stresses during freezing and drying steps. The freezing protocol and drying conditions have a significant impact on the quality parameters of the final product (4, 5).

It is now well known that various stages of lyophilization are based on very sound physical, chemical and engineering principles and can be controlled to the extent that the outcome of a given process performed on a given product can often be estimated to be within fairly close tolerance, without the need for trial-and-error experimentation (6). Even more important, stable freeze-dried nanoparticles can be designed by matching an optimum nanoparticle formulation with its associated optimum drying process cycle. In order to design an optimum nanoparticles freeze-drying process, process development scientists need to know the critical properties of the optimized formulation and how to apply this information to process design. The critical formulation properties include the glass transition temperature of the frozen sample ( $T_g'$ ), the collapse temperature of the formulation ( $T_c$ ), the stability of the nanoparticles and their encapsulated drug, and also the properties of the excipients used. The collapse temperature is the maximum allowable product temperature during primary drying (7). Freeze-dried product loses macroscopic structure and collapses during primary drying if it is heated to above the temperature of collapse ( $T_c$ ).

Freeze-drying as a drying method has many applications for nanoparticles technology. The literature contains many examples of such applications. The main use of freeze-drying is for improving long term nanoparticles stability. The transformation of colloidal suspension into solid form has the advantage of preventing particles aggregation, also the degradation of polymer forming nano particles and the leakage of encapsulated drug out of nanoparticles. Furthermore, freeze- drying could be transformed into another solid dosage form intended for different administration routes (parenteral, oral, nasal, or pulmonary).

Dry powder formulation of highly heat-sensitive materials such as proteins, peptides, and enzymes can be prepared using freeze-drying method. Nanoliposomal dry powder formulations with different aerodynamic properties have been prepared using different proportions of carriers, cryoprotectants, and antiadherents (8, 9). Freeze-dried dry powder formulations for pulmonary administration of therapeutic molecules such as budesonide, ketotifen, amphotericin B, leuprolide acetate, and levonorgestral have been formulated (8-10).

## **6.1 Methods**

### **6.1.1 Cryo Differential Scanning Calorimetric (Cryo-DSC) Studies**

Differential scanning calorimetry was performed on a Shimadzu Thermal Analyzer, DSC-60 equipped with a monitor and a computerized thermal analyzer system. The instrument was calibrated using indium as a reference standard. For DSC studies, an accurately weighed amount (4-5 mg) polymers were transferred to aluminium pans and were scanned between -75 to 200°C at a heating rate of 2°C/min below 30°C and then at 10°C/min up to 200°C under inert nitrogen atmosphere at a flow rate of 40 mL/min using empty aluminium pans as reference.

### **6.1.2 Lyophilization of Nanoplexes**

A generic description of industrial freeze-drying process is as follows: After vials are loaded to the shelf, they are cooled down to around 5°C by lowering the freeze-dryer shelf temperature. The freezing step is initiated by quickly cooling the shelves to the desired freezing temperature and holding the temperature constant for equilibration. An annealing step is sometimes included for crystallization of bulking agent, whereby the shelf temperature

is raised to near or above the formulation's glass transition temperature in the frozen state. Following freezing, primary drying is initiated by introducing vacuum in the chamber. Chamber pressure is reduced below the saturated vapor pressure of ice at the frozen product temperature. The difference between the vapor pressure of ice and the chamber pressure provides the driving force for sublimation. By maintaining the chamber under vacuum, the chamber pressure is constantly maintained below the saturated vapor pressure of ice and sublimation continues. When all frozen bulk water is removed via sublimation, primary drying is complete. At this point, there is still some bound unfrozen water remaining in the product that can be removed by desorption at higher temperatures experienced during secondary drying. Therefore, the shelf temperature is typically raised to ambient or higher temperatures at this stage and held until the desired residual moisture is achieved. At that point, secondary drying is also complete, and the freeze dryer has the provision to stopper the vials inside the chamber. The chamber is then aerated to partially break the vacuum prior to the stoppering of the vials. After the stoppering, the chamber vacuum is fully released before vials are unloaded.

**Protocol:** Developed formulations were lyophilized to impart physical stability to the siRNA polyplex and to develop dry powder for inhalation. Various types of carriers i.e. sucrose, lactose and trehalose were used at different ratio to optimize the lyophilization and to optimize the particle characteristic during freeze drying. Developed nanoplex formulation was diluted with nuclease free water to get 1  $\mu$ M concentration of siRNA. Cryoprotectants (40 mg/mL) were added to formulations and then filled into the 2 mL glass vial having 13 mm neck diameter. Vials were half stoppered with grey bromo butyl slotted rubber stoppers and kept on the shelf of lyophilizer. Polyplexes as well as lipoplexes were freeze-dried to  $-40^{\circ}\text{C}$  and dried under vacuum for various time period to optimize the particle characteristic of dry powder. Complete lyocycle describing freezing time, primary and secondary drying time, ramp and hold duration, vacuum level are given below in **Figure 6.1**. The lyophilized samples were then characterized for particle size, zeta potential, complexation efficiency and water content.

Initially, lyophilization was optimized for only one polyplex formulation i.e. AHP for selecting cryoprotectants based on aerosolization properties, particle size, zeta potential and physical appearance of the lyophilized cake and then same parameters were used for lyophilization of ALP, AAP and lipoplexes.

| Thermal Treatment Steps |      |      |           |
|-------------------------|------|------|-----------|
| Step #                  | Temp | Time | Ramp/Hold |
| Step # 1                | 5    | 30   | H         |
| Step # 2                | -40  | 120  | R         |
| Step # 3                | -40  | 300  | H         |
| Step # 4                | 0    | 0    | R         |
| Step # 5                | 0    | 0    | H         |
| Step # 6                | 0    | 0    | H         |
| Step # 7                | 0    | 0    | H         |
| Step # 8                | 0    | 0    | H         |
| Step # 9                | 0    | 0    | H         |
| Step # 10               | 0    | 0    | H         |
| Step # 11               | 0    | 0    | H         |
| Step # 12               | 0    | 0    | H         |

|                    |           |
|--------------------|-----------|
| Freeze Temp        | -40 °C    |
| Additional Freeze  | 0 min     |
| Condenser Setpoint | -60 °C    |
| Vacuum Setpoint    | 100 mTorr |

| Primary Drying Steps |      |      |     |           |
|----------------------|------|------|-----|-----------|
| Step #               | Temp | Time | Vac | Ramp/Hold |
| Step # 1             | -40  | 200  | 200 | H         |
| Step # 2             | -30  | 120  | 150 | R         |
| Step # 3             | -30  | 180  | 150 | H         |
| Step # 4             | -20  | 120  | 150 | R         |
| Step # 5             | -20  | 240  | 150 | H         |
| Step # 6             | -15  | 60   | 100 | R         |
| Step # 7             | -15  | 300  | 100 | H         |
| Step # 8             | -10  | 120  | 100 | R         |
| Step # 9             | -10  | 120  | 100 | H         |
| Step # 10            | 0    | 60   | 100 | R         |
| Step # 11            | 0    | 120  | 100 | H         |
| Step # 12            | 10   | 60   | 100 | R         |
| Step # 13            | 10   | 120  | 100 | H         |
| Step # 14            | 20   | 60   | 100 | R         |
| Step # 15            | 20   | 240  | 100 | H         |
| Step # 16            | 0    | 0    | 0   | H         |
| Post Heat            | 25   | 900  | 100 |           |

**Figure 6.1** Thermal Cycle for Freeze Drying

### 6.1.3 Residual Water Content

The residual water content of lyophilized liposomes was determined by Karl-Fischer titration (11). Commercially available pyridine free reagent was used for analysis. The reagent was standardized with addition and determination of known quantity of water (250 mg). Firstly, 40 mL of anhydrous methanol was added into the titration vessel and titrated with the reagent to remove any residual water in methanol. Following this, samples were added and water content was determined by titrating slowly with reagent.

#### **6.1.4 Particle Size and Zeta Potential:**

Obtained dry powder was rehydrated with nuclease free water and dilute appropriately. Particle size and zeta potential of rehydrated dry powder were measured as described in Chapter 5.

#### **6.1.5 Aerosolization Performance of the Formulations**

The dry powder was sieved subsequently through 120# and 240# sieves to get uniform and small particle size which can have maximum fine particle fraction with optimal MMAD. Aerosolization behaviour of the developed formulations was determined based on Mass median aerodynamic particle size using Andersen cascade impactor (ACI). Aerosolization performance of the developed dry powder formulations was determined by using previously developed method by Pfeifer et al. (12). In brief, powders used for this measurement contained Rhodamine B, which was added in 1 mM concentration to the suspension of nanoplexes containing appropriate amount of cryoprotectant prior to lyophilization in order to facilitate subsequent quantification.

##### **6.1.5.1 Spectrofluorometric Method for Detection of Rhodamine B**

In this study, we took fluorescence spectra of Rhodamine B in saline solution at room temperature in the concentrations range of 2 ng/mL to 20 ng/mL using a spectrofluorometer. Calibration curve of concentration against fluorescence intensity was plotted. Maximum excitation wavelength of 553 nm and maximum emission wavelength of 576 nm were used for the fluorescence measurement. Emission spectras were recorded from the wavelength above the excitation wavelength and upto 770 nm. Interference studies were performed to find out effect of lactose, sucrose and trehalose on known concentration of Rhodamine B.

##### **6.1.5.2 Aerodynamic Particle Size using Andersen Cascade Impactor (ACI)**

ACI is the instrument of choice as per regulatory bodies' requirements to determine aerodynamic particle size distribution of inhalation formulations. It operates on the principle of inertial impaction on each stage of impactor comprising series of jets through which sample laden air is drawn, with the help of vacuum, from the inhaler device. Stages are arranged in a stack in decreasing order of particle size. Particle mass below 5  $\mu\text{m}$  (range 1-5  $\mu\text{m}$ ) is usually described as the respirable fraction or fine powder fraction

(FPF) that actually settles in the lung. Bigger particles get impacted in oropharynx and particles below 1  $\mu\text{m}$  are exhaled as such without lung deposition. ACI was assembled and inhaler device (Aerolizer) was primed by connecting to the mouthpiece adapter for air-tight connection with induction port. Flow meter was attached to the induction port, pump was switched on and two way solenoid valve was opened to adjust the flow control valve to the desired flow rate. ACI was operated at 28.3 L/min flow rate to determine the aerodynamic particle size of the dry powder formulations. This was achieved by activating the timer (adjusted 10 sec to get 4 kPa to give an inspiration volume of 4L) on the Critical Flow Controller controlling the two way solenoid valve. Flow rate stability was ensured throughout the operation by measuring the absolute pressure at a point on either side of flow control valve. Ratio of pressures on either side should be  $\leq 0.5$  to ensure stable flow. Inhaler device was loaded with the capsule containing the dry powder formulation and connected to induction port via mouthpiece adapter. Among five capsules containing 20 mg of dry powder formulation, each were discharged into the apparatus one by one from Aerolizer device at appropriate flow rate by activating the timer to give a pressure drop of 4 kPa. At the end, samples were collected by rinsing the collection plates and walls of respective stages with saline. Analysis of the amount of fluorescence obtained on each stage was done to determine emitted dose (ED), fine powder fraction (FPF), Mass Median Aerodynamic Diameter (MMAD) and Geometric Standard Deviation (GSD). Recovered dose (RD) was determined as the total amount of dose recovered from the inhaler, capsule shell and the apparatus and was expressed as the percentage of the average assay amount.

ED was calculated as the amount emitted from the inhalation device and capsule into the apparatus.

FPD was considered as the amount of dose found below effective cut-off diameter  $< 4.7\mu$ . FPF was the ratio of FPD to RD.

Mass Median Aerodynamic Diameter MMAD is defined as the diameter at which 50% of the particles by mass are larger and 50% are smaller. USP <601> calls for determining the MMAD by plotting, on log probability paper, the cumulative percentages of mass less than the stated aerodynamic diameters versus the aerodynamic diameters. Dry powder retained on each stage was determined by using spectrofluorometer. Then cumulative percent fraction

containing less than each size range is determined. The MMAD is taken as the intersection of the line with the 50% cumulative percent. Computational methods can also be applied.

GSD is a measure of the spread of an aerodynamic particle size distribution. Typically calculated as follows:

$$\text{GSD} = (d_{84}/d_{16})^{1/2}$$

Where  $d_{84}$  and  $d_{16}$  represent the diameters at which 84% and 16% of the aerosol mass are contained, respectively, in diameters less than these diameters.

### **6.1.6 Integrity of siRNA**

Developed dry powder was rehydrated with small amount of nuclease free water and integrity of siRNA in developed dry powder for inhalation was determined as described in chapter 5.

### **6.1.7 X-ray Diffraction Studies (XRD)**

The main objective of this study was to determine possible changes in crystallinity of carrier after lyophilization.

## **6.2 Results and Discussion**

### **6.2.1 Cryo DSC**

Cryo-DSC was performed to check whether there was any decrease or increase in the glass transition temperature of PEI upon modification with Boc-amino acids. Also, the glass transition characteristics of modified polymers could be helpful in determining the lyophilization cycles for freeze-drying of the polyplex formulations thereof. As it can be seen from the **Figure 6.2**, PEI exhibited glass transition step at  $-52^{\circ}\text{C}$ . Due to its highly branched structure, it is completely amorphous. In contrast, copolymers clearly showed a shift of  $T_g$  to higher values in comparison to the  $T_g$  of homopolymer PEI, i.e.  $18^{\circ}\text{C}$ ,  $12^{\circ}\text{C}$  and  $16^{\circ}\text{C}$  for AA, AH and AL respectively (**Figure 6.3**, **Figure 6.4** and **Figure 6.5**). The shift of  $T_g$  to higher values is dependent on the amount of Boc amino acid substituted on PEI. In this case, the Boc amino acids is well mixed within the PEI and, therefore, can interact very well with the polyamine, thus resulting in a clear shift of the  $T_g$ .

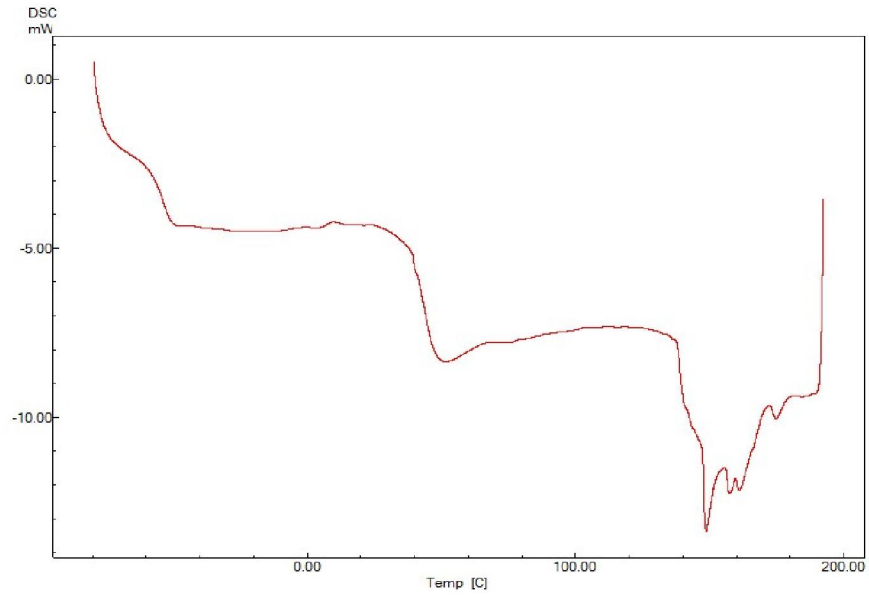


**Figure 6.2** DSC thermogram of PEI.

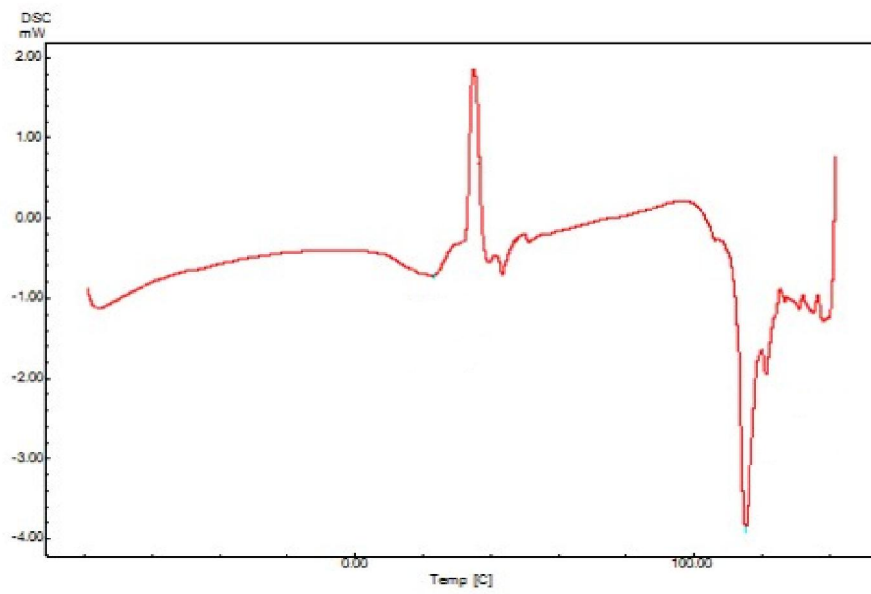


**Figure 6.3** DSC thermogram of AA.

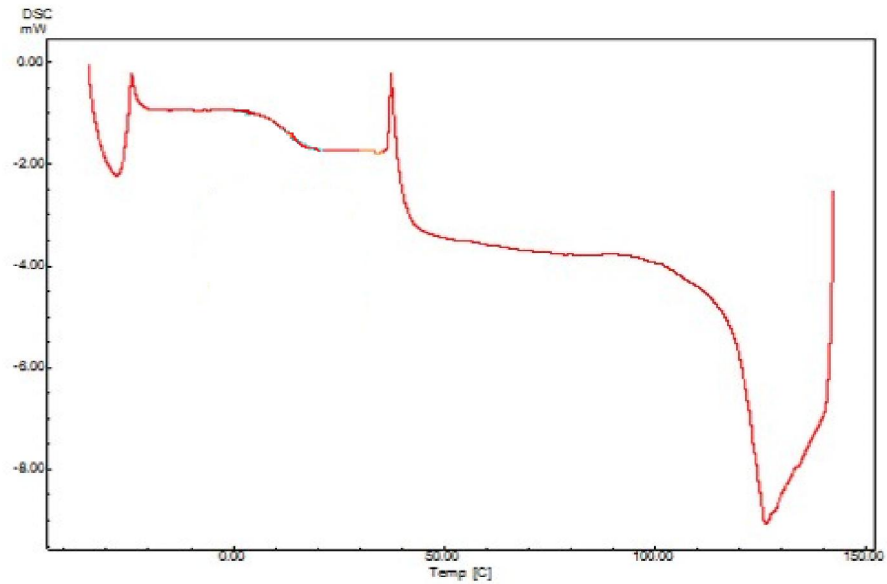


**Figure 6.4** DSC thermogram of AH.

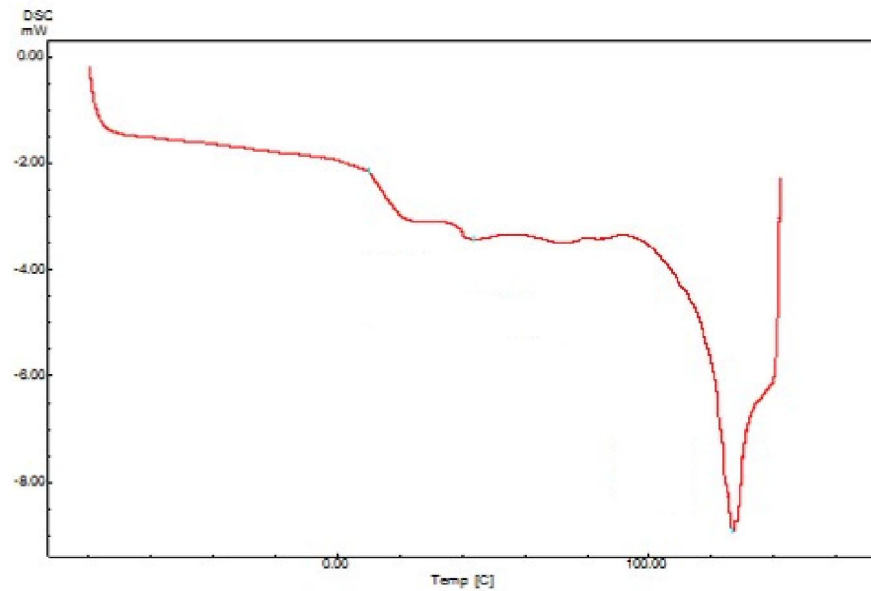


**Figure 6.5** DSC thermogram of AL.

Usually, high conductivity is observed in polymer complexes only when the temperature is above the glass transition temperature ( $T_g$ ), that is, above the temperature at which the substance changes from a solid to glassy state (the melting point of a polymer is usually above its glass transition temperature). Indications of the change of a polymer from solid to liquid are abrupt changes in certain properties, such as coefficient of expansion and heat capacity.

The physicochemical and mechanical properties of freeze dried products are temperature dependent and characteristic of the formulation composition. Below its glass transition temperature (defined as  $T_g'$ ), this amorphous phase exists as a "glass", which is a hard and brittle material with negligible mobility on practical timescales. The characteristic temperature at which motion begins, the  $T_g'$ , has been found to correlate strongly with the temperature at which the frozen cake undergoes collapse (13). Therefore, it is critical during primary drying to maintain the sample temperature below the  $T_g'$  of the formulation to prevent collapse of the cake. However, one may go for drying above  $T_g'$  after the primary drying phase has completed, as the cake is already formed and only bound water remains to be removed from sample.

### **6.2.2 Lyophilization of Nanoplexes**

Conversion of liquid dispersion of siRNA nanoplexes into dry powder was achieved by lyophilization. However, the process of lyophilization itself may lead to various physicochemical changes in the formulation i.e. aggregation and fusion of nanoparticulate formulations, loss of integrity, loss of siRNA complexation. Hence, in order to provide protection against detrimental effects of freezing and get a dry powder with good physical stability cryoprotectants were added to the formulation. **Figure 6.6** shows the thermal kinetic of product in comparison with shelf during the cycle of lyophilization.

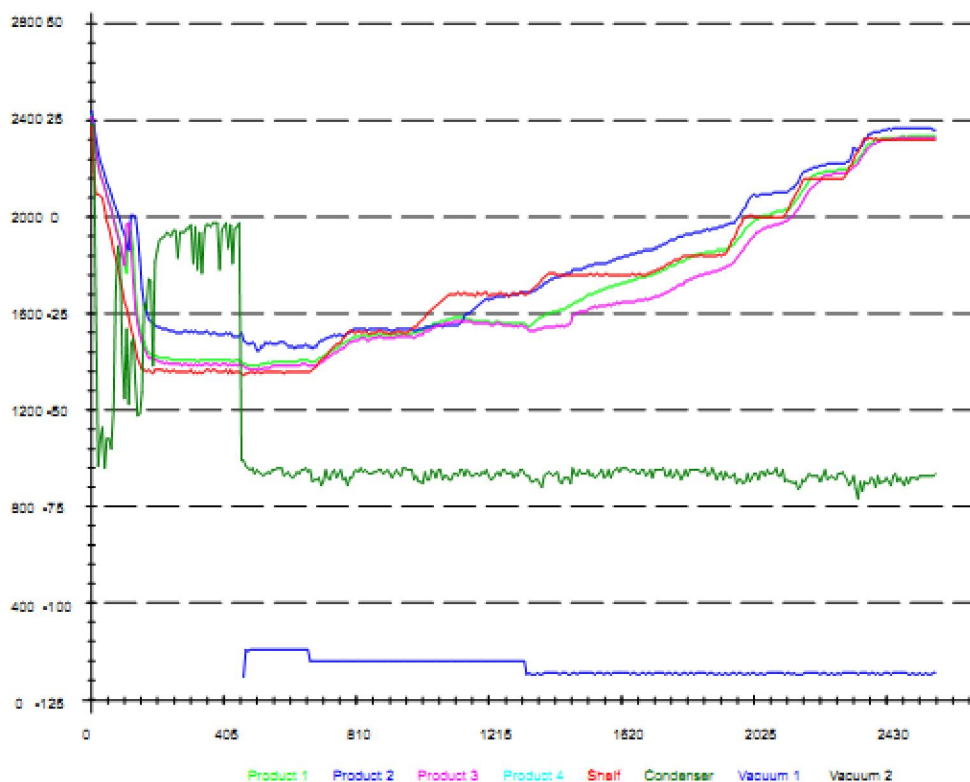


**Figure 6.6** Thermal graph of freeze drying cycle.

Different cryoprotectants were tried at the concentration of 40 mg/mL to AHP. Additionally, cryoprotectants concentration was chosen to function as a bulking agent and act as a carrier for the nanoplexes for successful delivery via pulmonary route. During freezing there is an ice formation from water molecules and this ice may affect the physical properties of complexes. Cryoprotectant helps to stabilize the system by providing the protection against developed local effects during freezing and also prevent increase in local concentration of the precipitated solid during freezing. These all collectively stabilize the nanomaterial in its much possible original form.

### 6.2.3 Particle Size, Zeta Potential and Moisture Content

Additionally, lyophilized formulation should retain their original characteristics on reconstitution. Hence, lyophilized formulations were tested for particle size, zeta potential and physical appearance on hydration of cake with nuclease free water. However, no degradation of siRNA was observed after lyophilization and also complexation was stable (**Table 6.1**).

**Table 6.1** Optimization of lyophilization for AHP

| Type of Cryoprotectant | Moisture Content (% W/W) | Before Lyophilization |                     | After Lyophilization |                     |
|------------------------|--------------------------|-----------------------|---------------------|----------------------|---------------------|
|                        |                          | Particle Size (nm)    | Zeta Potential (mV) | Particle Size (nm)   | Zeta Potential (mV) |
| Sucrose                | 1.65                     |                       |                     | 141.3±3.7            | 22.19±1.30          |
| Lactose                | 1.77                     | 137.6 ±4.3            | 20.45±1.96          | 138.5±2.5            | 21.85±2.20          |
| Trehalose              | 1.93                     |                       |                     | 145.4±4.3            | 21.76±1.65          |

\*Values are represented as mean±SD, n=3.

The lyophilization cycle for 42 hr provided the good physical properties of cake with good dispersibility. After lyophilization for 42 hr, water content in lyophilized product had water content of approximately 2%. Cryoprotectants i.e. lactose, sucrose and trehalose were able to preserve the particle size of siRNA formulations after 42 hr of lyophilization at concentration of 40 mg/mL. For all types of cryoprotectant, the zeta potential value did not change significantly. This result suggest the stability of complex after lyophilization and hence preservation of siRNA in the intact form. All used cryoprotectants preserved the particle size within narrow range as compared to non-lyophilized siRNA formulations. Dry powder formulation also has the same transfection efficiency as that of freshly prepared polyplexes. The developed powder was then characterized for performance on aerosolization. On the basis of fine particle fraction, the optimized cryoprotectants were selected for development of dry powder for all remaining nanoplexes i.e. ALP, AAP and nanoplexes and then characterized for particle size, zeta potential and moisture content (**Table 6.2**).

**Table 6.2** Lyophilization of AAP, ALP and lipoplex

| Nanoplex | Moisture Content (% W/W) | Before Lyophilization |                     | After Lyophilization |                     |
|----------|--------------------------|-----------------------|---------------------|----------------------|---------------------|
|          |                          | Particle Size (nm)    | Zeta Potential (mV) | Particle Size (nm)   | Zeta Potential (mV) |
| AAP      | 1.85                     | 152.5±5.7             | 14.03±1.90          | 157.4±4.88           | 14.15±1.76          |
| ALP      | 1.81                     | 168.3±5.1             | 14.33±2.21          | 173.5±3.93           | 14.29±2.33          |
| Lipoplex | 1.72                     | 118.8±4.7             | 27.95±2.3           | 121.4.4±4.67         | 26.84±2.32          |

\*Values are represented as mean±SD, n=3.

### 6.2.4 Spectrofluorometric Method for Detection of Rhodamine B

Rhodamine B was then used to verify the method for linearity. Calibration curve was obtained by plotting the graph of concentration of Rhodamine B Vs fluorescent intensity (**Figure 6.7** and **Figure 6.8**). The correlation coefficient obtained from the calibration curve was  $Y=25.972X+118.73$ . Data of % recovery and %relative standard deviation (**Table 6.3** and **Table 6.4**) showed the validity of the method and hence, can be used for further studies.

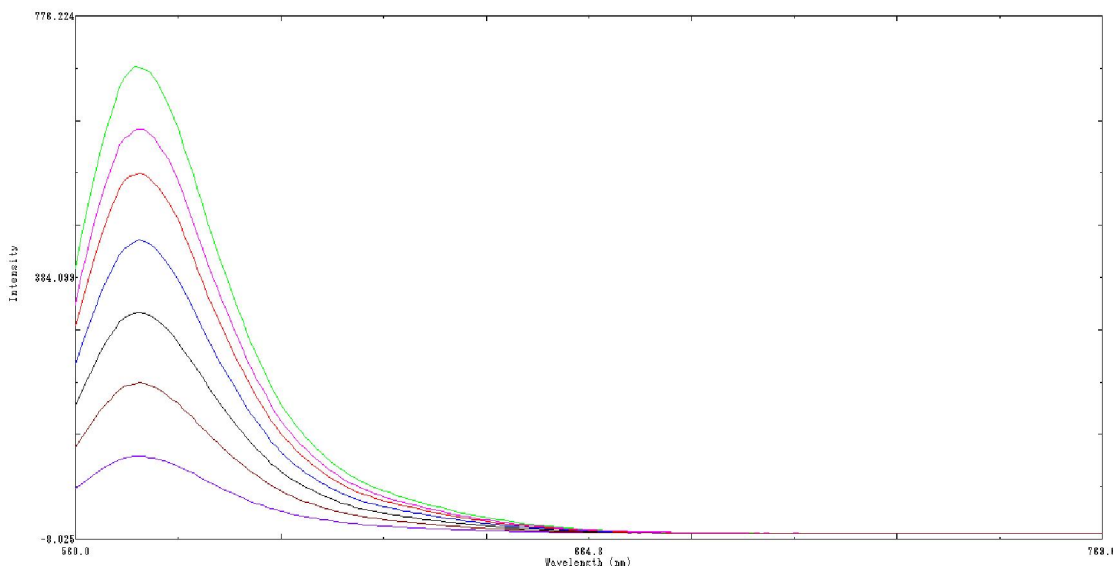


**Figure 6.7** Spectrofluorometric spectras of Rhodamine B.

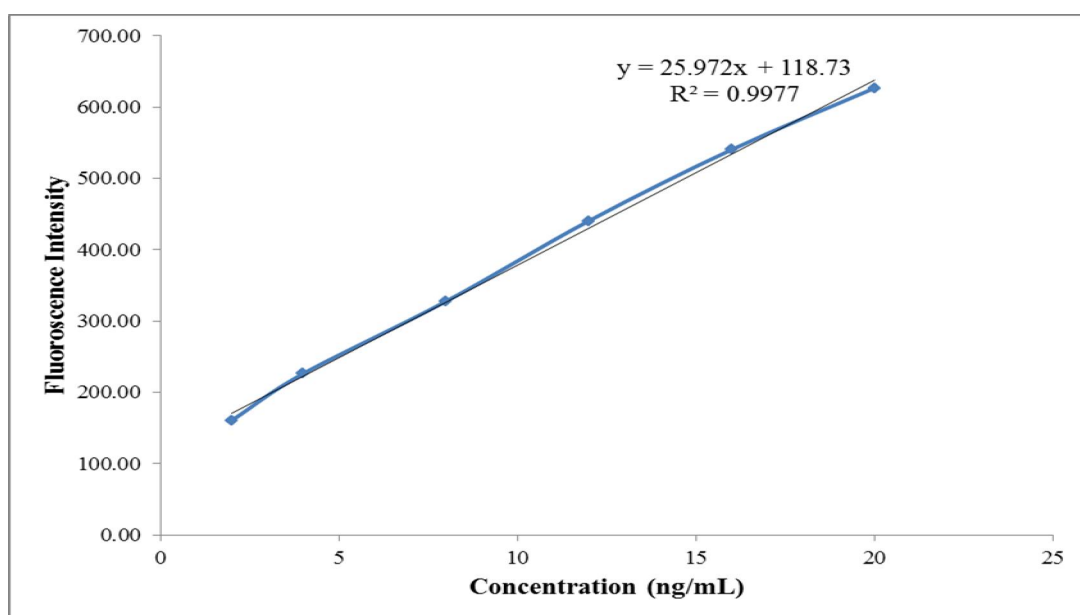


**Figure 6.8** Calibration curve for Rhodamine B

**Table 6.3** Results of accuracy measurements

| Actual Concentration (ng/mL) | Observed Concentration (ng/mL) | Standard Deviation (SD) | %Recovery |
|------------------------------|--------------------------------|-------------------------|-----------|
| 2                            | 1.96                           | 0.049                   | 98.18     |
| 12                           | 12.20                          | 0.114                   | 101.71    |
| 20                           | 19.61                          | 0.173                   | 98.06     |

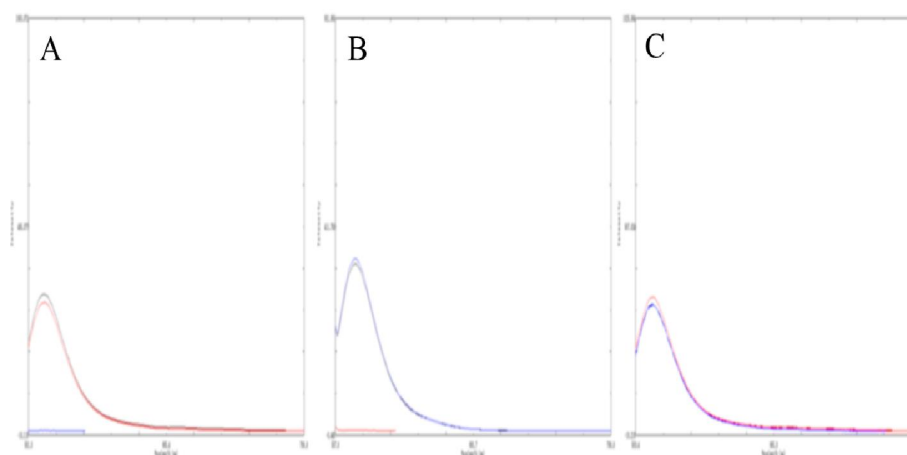
\*Values are represented as mean $\pm$ SD, n=3.

**Table 6.4** Intraday and Interday precision of the method

| Actual Concentration (ng/mL) | Observed Concentration $\pm$ SD |                    | %Relative Standard Deviation |                    |
|------------------------------|---------------------------------|--------------------|------------------------------|--------------------|
|                              | Intraday precision              | Interday Precision | Intraday precision           | Interday Precision |
| 2                            | 1.96 $\pm$ 0.049                | 1.96 $\pm$ 0.070   | 2.512                        | 3.56               |
| 12                           | 12.20 $\pm$ 0.114               | 12.22 $\pm$ 0.107  | 0.935                        | 0.597              |
| 20                           | 19.61 $\pm$ 0.173               | 19.62 $\pm$ 0.241  | 0.886                        | 0.996              |

\*Values are represented as mean $\pm$ SD i.e. n=9

No interference of lactose, sucrose and trehalose with known concentration of Rhodamine B (**Figure 6.9**) was found out and hence this Spectrofluorometric method was further used for analysis of aerosolization properties of developed dry powders for inhalation.

**Figure 6.9** Interference study of Rhodamine B with lactose(A), trehalose(B) and sucrose(C).

### 6.2.5 Aerosolization Performance of Dry Powder for Inhalation

Further, the formulations when tested on ACI under the standard conditions of USP, showed significant *in vitro* lung deposition. Dry powder formulations developed by using lactose showed higher fine particle fraction as compared to trehalose and sucrose and hence lactose was used as carrier for development of dry powder formulation of other nanoplexes. The FPF and MMAD of the tested formulations have been tabulated in **Table 6.5**.

**Table 6.5** Aerodynamic particle size of dry powder formulations.

| Sr No | Formulation | Cryoprotectant | Nomenclature | Emitted Dose (%) | MMAD ( $\mu\text{m}$ ) | GSD           | FPF (%)        |
|-------|-------------|----------------|--------------|------------------|------------------------|---------------|----------------|
| 1.    | AHP         | Lactose        | PDPI L1      | 87.14±<br>3.32   | 3.85±<br>0.19          | 2.18±<br>0.13 | 34.59<br>±2.1  |
| 2.    | AHP         | Sucrose        | PDPI S1      | 85.4±<br>3.35    | 4.33±<br>0.23          | 2.15±<br>0.15 | 25.29<br>±1.59 |
| 3.    | AHP         | Trehalose      | PDPI T1      | 86.2±<br>3.9     | 4.19±<br>0.19          | 2.43±<br>0.21 | 28.07<br>±1.87 |
| 4.    | AAP         | Lactose        | PDPI L2      | 88.2±<br>3.86    | 3.66±<br>0.17          | 2.29±<br>0.17 | 36.39<br>±1.6  |
| 5.    | ALP         | Lactose        | PDPI L3      | 89.3±<br>4.3     | 3.64±<br>0.15          | 2.20±<br>0.21 | 36.73<br>±1.76 |
| 6.    | DL          | Lactose        | LDPI         | 89.8±<br>2.4     | 3.67±<br>0.19          | 2.15±<br>0.23 | 37.19<br>±1.57 |

\*Values are represented as mean±SD i.e. n=3

Aerosolization properties of dry powder containing AHP showed that all of the three cryoprotectants can be used for pulmonary delivery of siRNA with more or less fine particle fraction. When we compare these cryoprotectants for aerosolization properties, then it was found that lactose have good ability to generate maximum fine particle fraction followed by trehalose and sucrose. Hence, lactose was used for the development of dry powder of all the remaining nanoplexes i.e. ALP, AAP and lipoplexes. We have selected the optimized carrier as a role model for development of dry powder of all nanoplexes because nanoplexes are having almost same physicochemical properties and are present in very low concentration as compared to cryoprotectants.

All the formulations developed by lactose and with their similar nanosized range of below 200 nm and almost same siRNA:lactose ratio showed similar deposition pattern with FPF in range of 34-37% and MMAD of 3.6-4  $\mu\text{m}$ . The MMAD of  $>4 \mu\text{m}$  indicates lung distribution in trachea, upper respiratory area and upper alveoli. When the powder comes in contact with lung fluids, siRNA nanoplexes will be detached from sugar moiety. These nanoplexes then can be internalized to give intracellular delivery as well as transfection efficiency.

In order to check whether dry powder formulations developed retained the siRNA integrity, developed formulations were compared with 10 bp ladder using heparin polyanion competition assay (**Chapter 5**). And as shown in **Figure 6.10**, all DPI formulaitons of nanoplexes retained the integrity of the siRNA.

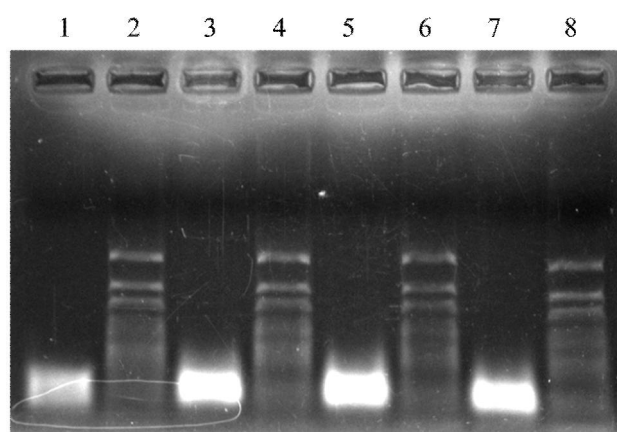


**Figure 6.10** Integrity of siRNA in dry powder formulations.

(Lane 1: PDPI L1, Lane 2: ladder, Lane 3: PDPI L2, Lane 4: ladder, Lane 5: PDPI L3, Lane 6:ladder, Lane 7:LDPI, Lane 8:ladder).

### 6.2.6 X-ray Diffraction Studies

XRD is one of the most sensitive and fool proof methods for solid-state characterization as the results are obtained directly from the atomic arrangements of the crystalline material. XRD results of dry powder formulation compared to placebo have been shown in the **Figure 6.11** and **Figure 6.12**. Various peaks at  $2\theta$  value were observed in X-Ray diffractograms of lactose (12.54, 19.55, 20.00, 20.83, 21.23, 26.59 and 37.56) which showed their crystalline nature. It is clear from the X-Ray diffractograms that there was a drastic change in the crystallinity of carrier after processing by freeze drying. Crystalline peaks at  $2\theta$  diffractograms of lactose were not seen in case of lyophilized dry powder. Dry powder

prepared by lyophilization yielded an amorphous mass, which is a desirable characteristic for dry powder formulations for inhalation.

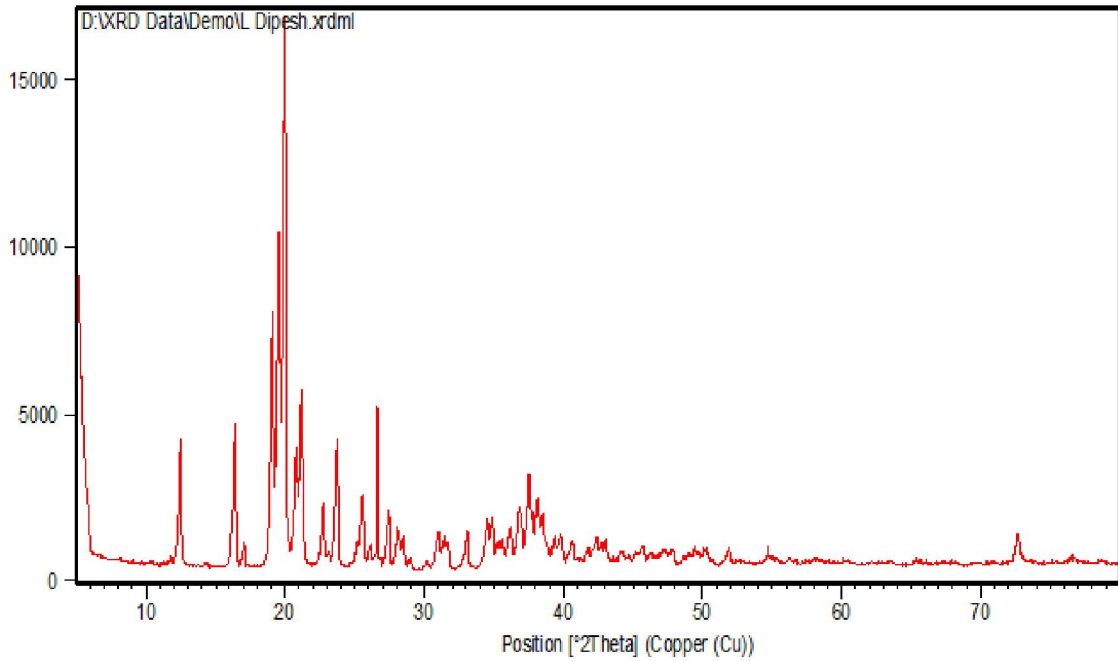


**Figure 6.11** X-Ray Diffractogram of Lactose

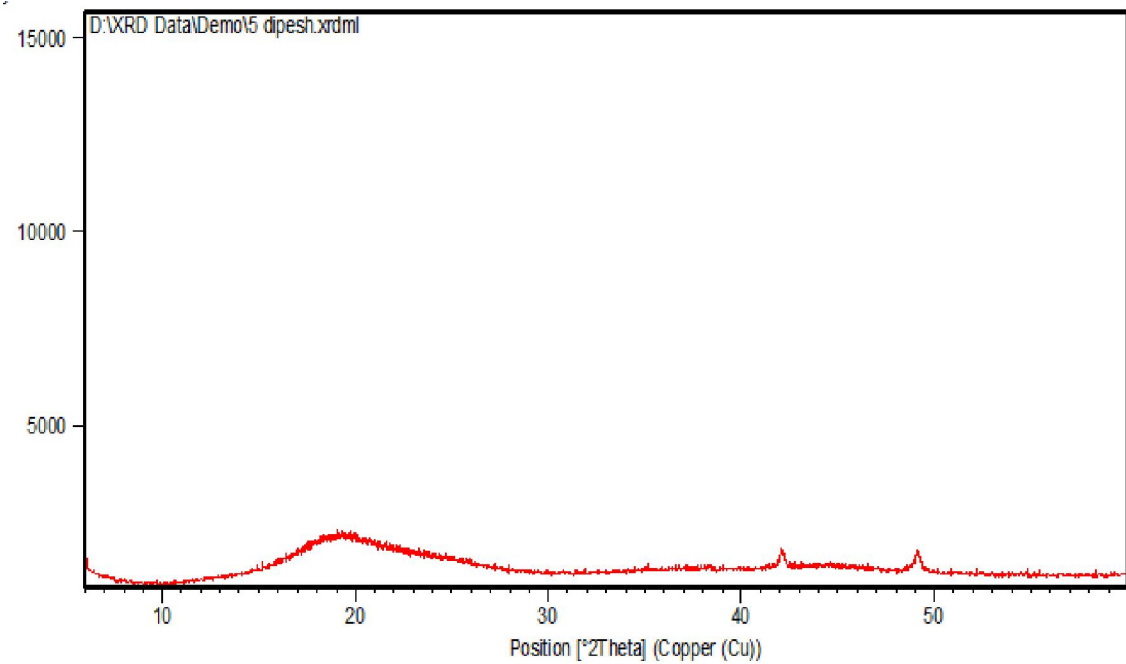


**Figure 6.12** X-Ray Diffractogram of PDPI L1

### **6.3 References**

1. Hottot A, Vessot S, Andrieu J. Determination of mass and heat transfer parameters during freeze-drying cycles of pharmaceutical products. *PDA J Pharm Sci Technol.* 2005;59(2):138-53.
2. Nakagawa K, Hottot A, Vessot S, Andrieu J. Influence of controlled nucleation by ultrasounds on ice morphology of frozen formulations for pharmaceutical proteins freeze-drying. *Chemical Engineering and Processing: Process Intensification.* 2006;45(9):783-91.
3. Daoussi R, Vessot S, Andrieu J, Monnier O. Sublimation kinetics and sublimation end-point times during freeze-drying of pharmaceutical active principle with organic co-solvent formulations. *Chemical Engineering Research and Design.* 2009;87(7):899-907.
4. Choi M-J, Hong G-P, Briançon S, Fessi H, Lee M-Y, Min S-G. Effect of a High-Pressure-Induced Freezing Process on the Stability of Freeze-Dried Nanocapsules. *Drying Technology.* 2008;26(10):1199-207.
5. Hawe A, Friess W. Impact of freezing procedure and annealing on the physico-chemical properties and the formation of mannitol hydrate in mannitol-sucrose-NaCl formulations. *Eur J Pharm Biopharm.* 2006;64(3):316-25.
6. Franks F. Freeze-drying of bioproducts: putting principles into practice. *European Journal of Pharmaceutics and Biopharmaceutics.* 1998;45(3):221-9.
7. Pikal MJ, Shah S, Roy ML, Putman R. The secondary drying stage of freeze drying: drying kinetics as a function of temperature and chamber pressure. *International Journal of Pharmaceutics.* 1990;60(3):203-7.
8. Shah SP, Misra A. Liposomal amikacin dry powder inhaler: effect of fines on in vitro performance. *AAPS PharmSciTech.* 2004;5(4):e65.
9. Shahiwala A, Misra A. Pulmonary absorption of liposomal levonorgestrel. *AAPS PharmSciTech.* 2004;5(1):E13.

10. Joshi M, Misra A. Dry powder inhalation of liposomal Ketotifen fumarate: formulation and characterization. *International Journal of Pharmaceutics*. 2001;223(1-2):15-27.
11. van Winden ECA, Crommelin DJA. Long term stability of freeze-dried, lyoprotected doxorubicin liposomes. *European Journal of Pharmaceutics and Biopharmaceutics*. 1997;43(3):295-307.
12. Pfeifer C, Hasenpusch G, Uezguen S, Aneja MK, Reinhardt D, Kirch J, et al. Dry powder aerosols of polyethylenimine (PEI)-based gene vectors mediate efficient gene delivery to the lung. *J Control Release*. 2011;154(1):69-76.
13. Pikal MJ, Shah S. The collapse temperature in freeze drying: Dependence on measurement methodology and rate of water removal from the glassy phase. *International Journal of Pharmaceutics*. 1990;62(2-3):165-86.